J Math Imaging Vis 25: 187–201, 2006

DOI: 10.1007/s10851-006-9696-7

A Shock-Capturing Algorithm for the Differential Equations of Dilation and Erosion

MICHAEL BREUß AND JOACHIM WEICKERT
Saarland University, Faculty of Mathematics and Computer Science, 66041 Saarbrücken, Germany
breuss@mia.uni-saarland.de
weickert@mia.uni-saarland.de

Published online: 21 September 2006

Abstract. Dilation and erosion are the fundamental operations in morphological image processing. Algorithms that exploit the formulation of these processes in terms of partial differential equations offer advantages for non-digitally scalable structuring elements and allow sub-pixel accuracy. However, the widely-used schemes from the literature suffer from significant blurring at discontinuities. We address this problem by developing a novel, flux corrected transport (FCT) type algorithm for morphological dilation/erosion with a flat disc. It uses the viscosity form of an upwind scheme in order to quantify the undesired diffusive effects. In a subsequent corrector step we compensate for these artifacts by means of a stabilised inverse diffusion process that requires a specific nonlinear multidimensional formulation. We prove a discrete maximum–minimum principle in this multidimensional framework. Our experiments show that the method gives a very sharp resolution of moving fronts, and it approximates rotation invariance very well.

Keywords: morphological dilation, morphological erosion, finite difference methods, flux corrected transport

1. Introduction

Mathematical morphology is concerned with image analysis of shapes. It is one of the oldest and most successful areas of digital image processing; see e.g. the textbooks [12, 17, 24, 30–32, 37] and the proceedings volumes [16, 18, 23, 27, 33, 34, 39] for an overview. Its fundamental operations are called *dilation* and *erosion*. For some greyscale image $f : \mathbb{R}^2 \to \mathbb{R}$ and a so-called structuring element $B \subset \mathbb{R}^2$, dilation and erosion are defined by

$$\textit{dilation:}\ (f \oplus B)(\mathbf{x}) := \sup\{f(\mathbf{x}-\mathbf{z}),\ \mathbf{z}\in B\}, \quad (1)$$

$$\textit{erosion:}\ (f \ominus B)(\mathbf{x}) := \inf\{f(\mathbf{x}+\mathbf{z}),\ \mathbf{z}\in B\}. \quad (2)$$

They form the basis of many other morphological processes such as openings, closings, top hats and morphological derivative operators.

While dilation and erosion are frequently implemented by algebraic set operations, for convex structuring elements there is also an alternative formulation in terms of partial differential equations (PDEs) [1, 2, 8, 40]. Let us consider a convex structuring element tB with a scaling parameter $t > 0$. Then, it can be shown that the calculation of $u(\mathbf{x}, t) = f \oplus tB$ and $u(\mathbf{x}, t) = f \ominus tB$ is equivalent to solving the PDEs

$$\partial_t u(\mathbf{x}, t) = \sup_{\mathbf{z}\in B} \langle \mathbf{z}, \nabla u(\mathbf{x}, t)\rangle, \quad (3)$$

$$\partial_t u(\mathbf{x}, t) = \inf_{\mathbf{z}\in B} \langle \mathbf{z}, \nabla u(\mathbf{x}, t)\rangle, \quad (4)$$

with f as initial condition [1, 29], respectively. Here, $\nabla = (\partial_x, \partial_y)^\top$ denotes the spatial nabla operator, and $\langle\cdot,\cdot\rangle$ is the Euclidean inner product. By choosing, e.g., a disc

$$B := \{\mathbf{z} \in \mathbb{R}^2,\ \|\mathbf{z}\|_2 \le 1\},$$

one obtains

$$\textit{dilation:} \quad \partial_t u = \|\nabla u\|_2, \tag{5}$$

$$\textit{erosion:} \quad \partial_t u = -\|\nabla u\|_2. \tag{6}$$

The solution at "time" t is the dilation (resp. erosion) of f with a disc of radius t and center 0 as structuring element. The Eqs. (5)–(6) need to be supplemented by an initial condition f with $f \in L_\infty(\mathbb{R}^2)$.

The dilation/erosion PDEs (5)–(6) belong to the class of so-called *hyperbolic* PDEs, see e.g. [13, 14] to learn more about partial differential equations. Hyperbolic processes decribe evolutions that propagate information with finite speed, similar as wave propagation. They may create shocks even if the initial data are smooth, and they require specific numerical schemes that take into account the propagation direction and handle shock-like discontinuities in a graceful manner [21]. Since many hyperbolic PDEs arise in computational fluid dynamics, it is natural to derive numerical methods for the dilation/erosion equations from techniques for hyperbolic conservation laws. In particular, finite difference methods such as the *Osher–Sethian schemes* [25, 26, 35] and the *Rouy–Tourin method* [28, 41] are widely-used in this context.

PDE-based algorithms for dilation/erosion offer two advantages over classical set-theoretic schemes [2, 10, 29]: first of all, they give excellent results for non-digitally scalable structuring elements whose shapes cannot be represented correctly on a discrete grid, for instance discs or ellipses. Secondly, the time t plays the role of a continuous scale parameter. Therefore, the size of a structuring element does not need to be multiples of the pixel size, and it is possible to get results with sub-pixel accuracy.

On the other hand, the main disadvantage of typical PDE-based algorithms for mathematical morphology consists of the fact that dissipative effects such as blurring of discontinuities occur. Apart from an investigation on the usefulness of high-order ENO[1] schemes [36,38], we are not aware of attempts in the literature to deal with these undesired *numerical diffusion* artifacts in PDE schemes for mathematical morphology.

It is the goal of the present paper to address this problem. For the development of our algorithm, we focus on the dilation process (5) since the erosion process can be treated analogously. We develop a new variant of the *flux corrected transport (FCT)* technique of Boris and Book [3–5, 19, 43] introduced in the context of fluid flow simulation. Our FCT scheme is used for approximating one- and two-dimensional morphological processes in an *accurate* and *rotationally invariant* fashion, an extension of the formulae we use to higher dimensions is straightforward. The aim of this paper is especially to give a detailed derivation and a sound mathematical basis for the general n-dimensional algorithm.

Related Work. The general idea behind the FCT technique is to compute in a first step the evolution with a scheme that may incorporate much numerical diffusion. Afterwards, this diffusion is annihilated in a proper fashion by applying a *stabilised inverse diffusion* step, sometimes also named *antidiffusion*. In conventional FCT methods, see especially [5], the amount of antidiffusion which is to be applied is basically determined by means of the so-called *modified equation* of the diffusive basis methods, see for instance [15,21] for details concerning this notion. In some newer works mainly concerned with finite element schemes, antidiffusion fluxes are computed by *algebraic* properties of the entries of corresponding stiffness matrices, see e.g. [20] and the references therein. We employ a different approach motivated by the theory of numerical methods for conservation laws, compare e.g. [15]: we construct our FCT scheme considering the *viscosity form* of the underlying method. By the use of this form we can effectively eliminate the influence of the numerical viscosity due to the spatial derivative. It turns out that our scheme provides a much sharper resolution in comparison with the schemes proposed by Osher and Sethian [26]. Let us note that in contrast to the classical works of Boris, Book and their collaborators, we derive the essential information for our algorithms on the *discrete* basis, while compared to the approach of Kuzmin and Turek [20] our proceeding is technically relatively simple.

Furthermore, both mentioned FCT approaches rely on an underlying *additive splitting* of the backward diffusion into fluxes between computational nodes: especially in the multidimensional case, the mentioned works proceed along the considerations of Zalesak [42]. In contrast, our *genuinely multidimensional* approach yielding directly the desired rotational invariance uses the dimensional dependent nonlinear form of the numerical viscosity. This proceeding is to our knowledge not explored up to now within the literature. However, its usefulness and simplicity is immediately evident in the image processing context presented here.

The algorithm we develop in our paper is close in spirit to a recent conference contribution by us, where we developed a FCT approach for three

one-dimensional model equations for numerical conservation laws [7]. However, it should be noted that the dilation/erosion PDEs we are investigating in our present paper cannot be written in conservation form, and that we do not restrict ourselves to the 1–D case.

Organisation of the Paper. Our paper is organised as follows. In the next section we introduce our novel FCT scheme for the dilation process in the 1-D case, where we describe the upwind scheme as predictor, and introduce an inverse diffusion algorithm as corrector. We illustrate its behaviour by an experiment and establish stability results in terms of a maximum principle. Section 4 extends these investigations to the 2-D case, and we consider some 2-D numerical tests. The paper is concluded with a summary in Section 5.

2. Existing Algorithms

As already meantioned, prominent PDE-based algorithms for the dilation equation are the first- and second-order methods of Osher and Sethian [25, 26, 35], and the first-order scheme of Rouy and Tourin [28, 41], see also [9, 22] for related work and discussions.

For the dilation equation

$$\partial_t u \;=\; \|\nabla u\|_2 \;=\; \left((\partial_x u)^2 + (\partial_y u)^2\right)^{1/2} \qquad (7)$$

the Rouy–Tourin scheme is given by

$$\begin{aligned} U_{i,j}^{n+1} &= U_{i,j}^n + \lambda\Big(\big(\max\big(0,\, U_{i+1,j}^n - U_{i,j}^n,\, U_{i-1,j}^n - U_{i,j}^n\big)\big)^2 \\ &\quad + \big(\max\big(0,\, U_{i,j+1}^n - U_{i,j}^n,\, U_{i,j-1}^n - U_{i,j}^n\big)\big)^2\Big)^{1/2}, \end{aligned} \qquad (8)$$

and the first-order Osher–Sethian upwind scheme can be written as

$$\begin{aligned} U_{i,j}^{n+1} = U_{i,j}^n \;+\; \lambda\, \Big(&\big(\max\big(0,\, U_{i+1,j}^n - U_{i,j}^n\big)\big)^2 \\ &+\big(\max\big(0,\, U_{i-1,j}^n - U_{i,j}^n\big)\big)^2 \\ &+\big(\max\big(0,\, U_{i,j+1}^n - U_{i,j}^n\big)\big)^2 \\ &+\big(\max\big(0,\, U_{i,j-1}^n - U_{i,j}^n\big)\big)^2\Big)^{1/2}. \end{aligned} \qquad (9)$$

Thereby, we use as in the following the notation U for discrete data, in contrast to the analytical solution u, and we denote the ratio of mesh sizes Δt and Δx in t and x direction by $\lambda = \Delta t/\Delta x$. We assume that $\Delta x = \Delta y$. The upper index k in $U_{l,m}^k$ denotes as usual the temporal level $k\Delta t$ while, analogously, the lower indices $l, m \in \mathbf{Z}$ specify the spatial mesh point $(l\Delta x, m\Delta y)$.

Table 1. Average L_1-errors of numerical solutions approximating the true solution given in Fig. 1(b). The grey value range is from 0 to 255.

Scheme	Average L_1-error per pixel
Osher–Sethian 1st order	4.66
Osher–Sethian 2nd order	4.76
new FCT	0.96

As indicated, the mentioned work of Osher and Sethian does not only deal with first-order upwinding, it also allows high-order variations. However, computational results are in the dilation/erosion case in practice comparable to the results of first-order integration, see Table 1, and thus we do not discuss high-order variants here.

We test the mentioned approaches comparing already with the scheme developed in this paper by use of a scenario that is sensitive to failures in the rotational invariance of a method, namely the dilation of a disc. Figure 1(a) shows the initial value of the dilation process, given by a representation of an exact circle with a radius corresponding to exactly 25 pixels (computed by subdividing each pixel into 100×100 subpixels and integrating the arising contributions). The circle is supposed to grow in a uniform fashion while the circular shape is preserved; the exact solution where the radius has grown by 10 pixels is shown in Fig. 1(b). In Fig. 1(c) we see the initial image evolved by the Osher–Sethian algorithm yielding a rotationally invariant, but somewhat blurred solution. The result of the Rouy–Tourin method is identical for this case (they are both identical in this test case to first-order upwinding). By Fig. 1(d) we give in comparison the result from the new FCT method we describe in this work. In order to assess the quality of the methods, we also give in Table 1 the L_1-errors between exact and computed solutions, including the one we obtain by use of the second-order scheme of Osher and Sethian (not displayed here as it is not substantially different than the first-order solution) where we have used for time integration as proposed in [26] the method of Heun.

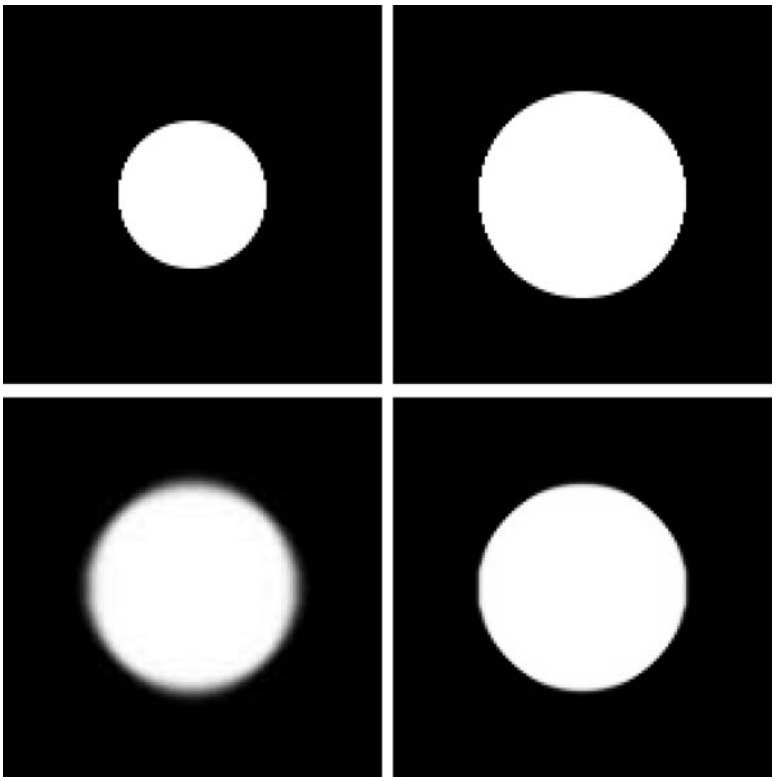

Figure 1. (a) Top left: Initial image, 128×128 pixels. (b) Top right: Dilated image. (c) Bottom left: Dilation by the first-order upwind scheme ($\Delta x = \Delta y = 1$, $\Delta t = 0.5$, 20 iteration). (d) Bottom right: Dilation by the new FCT scheme developed in the following (same parameters).

3. The One-Dimensional FCT Algorithm

We start our one-dimensional investigations in this section with a review of the essential properties of an upwind scheme for a general hyperbolic first-order PDE. Afterwards, we derive its specific structure for the case of a dilation equation and identify it with the Rouy–Tourin scheme. This scheme serves as first step in our FCT algorithm. In a second step we construct a suitable inverse diffusion step in order to compensate for the numerical viscosity that has been introduced by the upwind scheme. Finally we prove a discrete maximum principle for the FCT scheme.

3.1. The General Upwind Scheme in 1-D

The underlying method for our new FCT technique is the classical *upwind scheme*. For a general one-dimensional hyperbolic first-order PDE $u_t + (f(u))_x = 0$ with $f'(.) \geq 0$ it can be written as

$$U_j^{n+1} = U_j^n - \lambda \left(f\left(U_j^n\right) - f\left(U_{j-1}^n\right) \right) \qquad (10)$$

with the notations from the previous section. If $f'(.) < 0$ the upwind scheme is given by

$$U_j^{n+1} = U_j^n - \lambda \left(f\left(U_{j+1}^n\right) - f\left(U_j^n\right) \right). \qquad (11)$$

The upwind scheme has a number of favourable *stability properties*, i.e., the scheme mimics important properties of the underlying PDE on the discrete level. They can be summarised as follows:

Proposition 3.1 (Stability Properties of the Upwind Scheme). *Under the usual CFL stability condition,*[2] *the upwind scheme is a local extremum diminishing (LED) scheme. It does not introduce new extrema during a computation, i.e., it diminishes also the number of extrema (NED property). Moreover, the upwind scheme satisfies a discrete maximum–minimum principle: for all indices j and n in use holds*

$$\min_i \left(U_i^0\right) \leq U_j^n \leq \max_i \left(U_i^0\right).$$

Let us note, that stability in terms of a minimum-maximum principle is strongly linked to stability in the L_∞-norm. It is a useful concept in the nonlinear setting, which we need to address in the case of the PDEs of dilation/erosion, where classical stability notions as von Neumann-stability are no longer applicable. Moreover, in the context of image analysis, it implies that no over- and undershoots can occur. The proofs of the validity of the mentioned properties of the upwind scheme are simple, see for instance [7, 15] in the context of numerical schemes for conservation laws.

While the upwind scheme can also be shown to approximate the entropy solution[3] of the underlying PDE, it has a severe disadvantage: it suffers from undesirable blurring effects aka *numerical viscosity*. To quantify these viscous artifacts we write the scheme (10) in its *viscosity form*, i.e.,

$$U_j^{n+1} = U_j^n - \frac{\lambda}{2}\big(f(U_{j+1}^n) - f(U_{j-1}^n)\big) \tag{12}$$

$$+\frac{Q_{j+1/2}^n}{2}(U_{j+1}^n - U_j^n) - \frac{Q_{j-1/2}^n}{2}(U_j^n - U_{j-1}^n). \tag{13}$$

The basic idea behind this decomposition is to consider the part (12) of the method as a second-order approximation in space (and first order in time) of the underlying process, while part (13) is (in leading order) the discrete counterpart of the numerical diffusion incorporated in the scheme introduced by the spatial approximation.

One easily verifies that (10), (12) and (13) can be made identical by choosing viscosity coefficients $Q_{j+1/2}^n$ and $Q_{j-1/2}^n$ that satisfy

$$Q_{j+1/2}^n = \lambda\,\frac{f_{j+1}^n - f_j^n}{U_{j+1}^n - U_j^n} \qquad \text{and}$$

$$Q_{j-1/2}^n = \lambda\,\frac{f_j^n - f_{j-1}^n}{U_j^n - U_{j-1}^n} \tag{14}$$

for $U_{k+1}^n \neq U_k^n$, $k \in \{j,\ j-1\}$, and $f_i^l := f(U_i^l)$. By the prerequisite $f'(.) \geq 0$ necessary to apply an upwinding in the fashion (10), it is ensured that the viscosities $Q_{j\pm1/2}^n$ are nonnegative. The resulting numerical diffusion is responsible for undesirable blurring effects that are observed with this first-order method. Exactly the terms corresponding to (13), (14) will be negated in a suitable way during a subsequent, stabilised inverse diffusion step of the FCT routine.

Let us note that, although the viscosities $Q_{j\pm1/2}^n$ in (14) are nonlinear for general f, we will see that in the case of dilation and erosion processes they are in fact simply constants determined by the chosen space-time mesh. Nonlinear effects arise due to the required invariance under rotations as will be discussed in the section on the 2-D model.

3.2. The FCT Scheme for 1-D Dilation

We now derive the 1-D algorithm for dilation. The corresponding scheme for erosion can be constructed and discussed analogously.

3.2.1. The Formulation of the 1-D Upwind Basis Scheme. Let us define abbreviate notions for the *one-sided discrete differences*

$$\Delta U_{j+1/2}^k := U_{j+1}^k - U_j^k \tag{15}$$

and for the *centered discrete differences*

$$\Delta U_j^k := U_{j+1}^k - U_{j-1}^k. \tag{16}$$

In order to clarify the basic idea, let us point out explicitly, that a proper scheme describing the dilation process (5) satisfies the following

Principle 3.1 (Discrete Evolution Principle of the Dilation Process). *In order to reflect the properties of the analytical dilation operator, the following properties need to be satisfied on the discrete level:*

- *In regions of* (*strictly*) *monotone data, the flow is directed from lower to higher grey values.*
- *Local minima are increased, while local maxima are maintained.*

For the development of our 1-D algorithm, it is useful to fix the attention to a particular spatial index j and to consider a diversion of cases with respect to the data situations one may encounter.

Case 1. $\Delta U_{j-1/2}^n \geq 0$ and $\Delta U_{j+1/2}^n > 0$.

For this case, the upwind scheme and its viscosity form read

$$\begin{aligned} U_j^{n+1} &= U_j^n + \lambda\left(U_{j+1}^n - U_j^n\right) \\ &= U_j^n + \underbrace{\frac{\lambda}{2}\left(U_{j+1}^n - U_{j-1}^n\right)}_{(a)} \\ &\quad + \underbrace{\frac{\lambda}{2}\left(U_{j+1}^n - U_j^n\right) - \frac{\lambda}{2}\left(U_j^n - U_{j-1}^n\right)}_{(b)}. \end{aligned} \tag{17}$$

As indicated, (17)(a) is a second-order accurate approximation of $\Delta t\,|u_x|$, while (17)(b) implies $Q_{j\pm1/2}^n = \lambda$ in the investigated case.

Case 2. $\Delta U_{j-1/2}^n < 0$ and $\Delta U_{j+1/2}^n \le 0$.

Here the upwind scheme and its viscosity form read

$$\begin{aligned} U_j^{n+1} &= U_j^n + \lambda\left(U_{j-1}^n - U_j^n\right) \\ &= U_j^n + \frac{\lambda}{2}\left(U_{j-1}^n - U_{j+1}^n\right) \\ &\quad + \frac{\lambda}{2}\left(U_{j+1}^n - U_j^n\right) - \frac{\lambda}{2}\left(U_j^n - U_{j-1}^n\right), \end{aligned} \tag{18}$$

revealing the same structure as in (17), but the approximation of $\Delta t\,|u_x|$ is different here.

Case 3. $\Delta U_{j-1/2}^n < 0$ and $\Delta U_{j+1/2}^n \ge 0$.

The investigated case especially incorporates the situation

$$\Delta U_{j-1/2}^n < 0 \;\text{ and }\; \Delta U_{j+1/2}^n > 0,$$

i.e., a local minimum is located at the index j. Analogously to the proceeding within the Rouy–Tourin algorithm [28, 41], we choose the direction of the dilation flow according to the largest gradient, i.e.,

$$\begin{aligned} U_j^{n+1} &= U_j^n + \lambda \underbrace{\max\left(U_{j+1}^n - U_j^n,\, U_{j-1}^n - U_j^n\right)}_{:=\tilde{\Delta}U_j^n} \\ &= \begin{cases} U_j^n + \frac{\lambda}{2}\Delta U_j^n + \frac{\lambda}{2}\Delta U_{j+1/2}^n - \frac{\lambda}{2}\Delta U_{j-1/2}^n \\ \quad \text{if} \quad \tilde{\Delta}U_j^n = U_{j+1}^n - U_j^n, \\ U_j^n - \frac{\lambda}{2}\Delta U_j^n + \frac{\lambda}{2}\Delta U_{j+1/2}^n - \frac{\lambda}{2}\Delta U_{j-1/2}^n \\ \quad \text{if} \quad \tilde{\Delta}U_j^n = U_{j-1}^n - U_j^n. \end{cases} \end{aligned} \tag{19}$$

Note that this choice is not simply a matter of discrete modeling, it is also perfectly reasonable since

$$\pm\frac{\lambda}{2}\Delta U_j^n = \frac{\lambda}{2}\left(U_{j\pm1}^n - U_{j\mp1}^n\right) \approx \Delta t|u_x| \quad \text{for } \tilde{\Delta}U_j^n = U_{j\pm1}^n - U_j^n$$

is also a second-order accurate approximation of the dilation process at a local minimum of the data.

Case 4. $\Delta U_{j-1/2}^n \ge 0$ and $\Delta U_{j+1/2}^n \le 0$.

Here, according to the formulated Principle 3.1, we set

$$U_j^{n+1} := U_j^n. \tag{20}$$

Summary of Cases I to IV: Having finished the consideration of all possible cases, we can formulate the upwind scheme as follows:

$$U_j^{n+1} = \begin{cases} U_j^n \quad \text{for} \quad \Delta U_{j-1/2}^n \ge 0,\, \Delta U_{j+1/2}^n \le 0, \\ U_j^n + \frac{\lambda}{2}\left|\Delta U_j^n\right| + \frac{\lambda}{2}\Delta U_{j+1/2}^n - \frac{\lambda}{2}\Delta U_{j-1/2}^n, \;\text{ else.} \end{cases} \tag{21}$$

The scheme (21) is, because of its treatment of local minima, identical with the 1-D version of the already mentioned Rouy–Tourin method, which is derived in a completely different fashion for the 2-D case. Thereby, for the 1-D case, the CFL stability condition reads $\Delta t \le \Delta x$.

By the form (21) we have gained that we can identify the incorporated numerical viscosity arising by our approximation of the spatial derivative. Neglecting the influence of the first-order temporal approximation, we refer to the viscosity identified in the above fashion as the *numerical viscosity* of our scheme.

In order to illuminate the properties of the method (21), we apply it without further modification at a simple 1-D test problem depicted in Fig. 2. We clearly observe the desired dilation process, however, the numerical solution is fairly blurry.

3.2.2. The 1-D FCT Step. Now we turn to the FCT methodology. For this, we use in the following the data notions:

- $U_j^{n+1/2}$ for the data obtained by the upwind scheme starting from U_j^n,
- U_j^{n+1} for the data obtained after the inverse diffusion step.

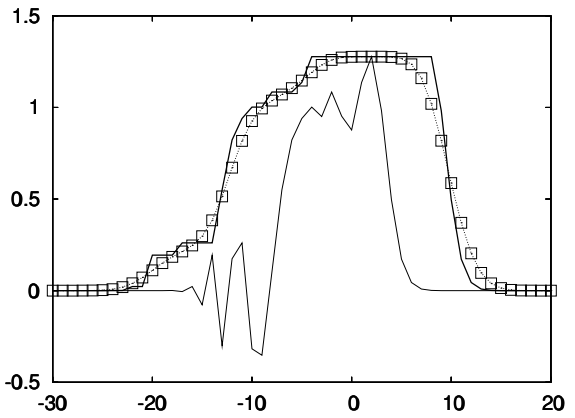

Figure 2. Oscillatory initial data and its dilation computed using the described first-order upwind scheme (21) ($\Delta x = 1$, $\Delta t = 0.4$, 15 iterations).

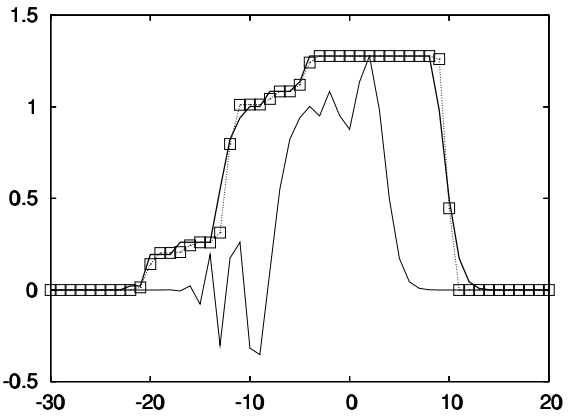

Figure 3. Oscillatory initial data together with (continuous line) the exact solution of the dilation process and (boxes) the new FCT scheme ($\Delta x = 1$, $\Delta t = 0.4$, 15 iterations).

When applying an inverse diffusion algorithm, it is evident that one has to incorporate a means of stabilisation. We would like to mention the

Principle 3.2 (of Boris and Book [3]). *No antidiffusive flux transfer of mass can push the density value at any grid point beyond the density value at neighboring points.*

The traditional FCT scheme realises this principle by computing antidiffusive fluxes $\tilde{g}_{j\pm1/2}$, so that

$$U_j^{n+1} = U_j^{n+1/2} - \tilde{g}_{j+1/2} + \tilde{g}_{j-1/2} \tag{22}$$

follows. Thereby, Boris and Book use

$$\tilde{g}_{j+1/2} := \text{minmod}\left(\Delta U_{j-1/2}^{n+1/2}, \eta_{j+1/2}\Delta U_{j+1/2}^{n+1/2}, \Delta U_{j+3/2}^{n+1/2}\right), \tag{23}$$

$$\text{minmod(a, b, c)} := \text{sign}\,(b)\max(0, \min(\text{sign}\,(\text{b})\text{a}, |\text{b}|, \text{sign}\,(\text{b})\text{c})), \tag{24}$$

where $\eta_{j+1/2}$ is obtained by an analysis of the *modified equation*, i.e., it is determined on the differential level; see especially [5].

In 1-D, our proceeding is similar. However, we negate as indicated the diffusion computed by the discrete *viscosity form* introduced before.

Thus, we realize Principle 3.2 ensuring the stability of the backward diffusion step by introducing stabilised inverse diffusion terms of type

$$g_{j+1/2} := \text{minmod}\Big(\Delta U_{j-1/2}^{n+1/2}, \frac{\lambda}{2}\Delta U_{j+1/2}^{n+1/2}, \Delta U_{j+3/2}^{n+1/2}\Big) \tag{25}$$

leading here, i.e., in 1-D, to the correction formula

$$U_j^{n+1} = U_j^{n+1/2} - g_{j+1/2} + g_{j-1/2}. \tag{26}$$

Thereby, in (25), as the index of g indicates, the middle argument of the minmod-function corresponds to the viscous flux between the cells j and $j+1$ as identified by our previous analysis, while the left and right arguments are responsible for stabilisation. For a more detailed analysis of the role of the minmod-function, see [6].

We can apply our FCT algorithm incorporating (i) the evolution step performed by the method (21) and (ii) the correction step (26) again at our 1-D test case. For the same computational parameters as before, we see in Fig. 3 the initial data together with the solution obtained using the new FCT scheme. Note the sharp profiles of discontinuities obtained using the latter method while the location of fronts is captured correctly due to the properties of the underlying upwind scheme.

Let us remark, that due to the use of the upwind scheme as basis method, some viscous arefacts inevitably survive, e.g., in the presence of gaps, see Fig. 4. The gap displayed there has a width of 11 pixels, and thus the exact solution at $t = 5$ features a gap of exactly one pixel. However, at $t = 5$ the computed solution has

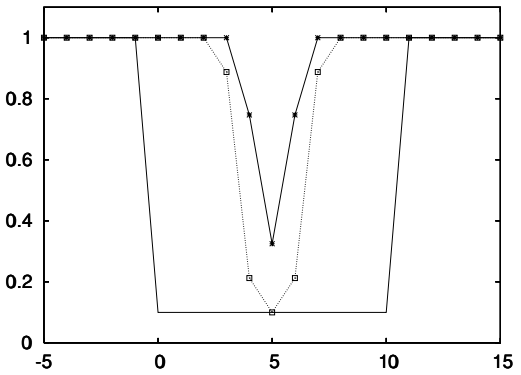

Figure 4. Initial data describing a gap, together with computed results using the new FCT scheme at (squares) $t = 4$ and (stars) $t = 5$, respectively ($\Delta x = 1$, $\Delta t = 0.5$).

already closed it to some degree. This is the price one has to pay for the correct propagation described by upwinding.

3.2.3. Stability of the 1-D FCT Scheme. In the context of morphological dilation processes, useful stability notions are a *global discrete maximum principle* as well as a *local discrete extremum principle*. We do not deal explicitly with minima since these are treated by the construction of the method in the usual fashion, increasing them. We proceed with the

Proposition 3.2 *(*Local Extremum Principle*).* *Let*

$$\operatorname{sign}\left(\Delta U_{k+1/2}^{n+1/2}\right) = \operatorname{sign}\left(\Delta U_{k-1/2}^{n+1/2}\right) \neq 0 \quad (27)$$

hold. Then the FCT scheme defined by

$$U_j^{n+1} = U_j^{n+1/2} - g_{j+1/2} + g_{j-1/2} \quad (28)$$

using g from (25) *satisfies locally a discrete maximum–minimum principle:*

$$U_j^{n+1} \;\geq\; \min\left(U_{j-2}^n,\, U_{j-1}^n,\, U_j^n,\, U_{j+1}^n,\, U_{j+2}^n\right) \quad (29)$$

and

$$U_j^{n+1} \;\leq\; \max\left(U_{j-2}^n,\, U_{j-1}^n,\, U_j^n,\, U_{j+1}^n,\, U_{j+2}^n\right). \quad (30)$$

Proof: Since the upwind basic scheme satisfies a discrete maximum–minimum principle, is is sufficient to show the validity of

$$U_k^{n+1} \in \operatorname{conv}\left(U_{k-1}^{n+1/2},\, U_k^{n+1/2},\, U_{k+1}^{n+1/2}\right)$$

where the convex hull conv denotes the set of all convex combinations:

$$U_k^{n+1} \in \sum_{i=-1}^{1} \alpha_i U_{k+i}^{n+1/2}, \quad \sum_{i=-1}^{1} \alpha_i = 1, \quad \alpha_i \geq 0.$$

The crucial observation is, that for the assumption (27) the flux contributions

$$-g_{j+1/2} \quad \text{and} \quad +g_{j-1/2}$$

defined by (25) have opposite sign, i.e., even if, for instance, in the case $U_j^{n+1/2} > U_{j-1}^{n+1/2}$, we have within the estimation

$$\begin{aligned} U_j^{n+1/2} - g_{j+1/2} &\geq U_j^{n+1/2} - \Delta U_{j-1/2}^{n+1/2} \\ &= U_j^{n+1/2} - \left(U_j^{n+1/2} - U_{j-1}^{n+1/2}\right) = U_{j-1}^{n+1/2} \end{aligned}$$

in the worst case the validity of the exact equality

$$U_j^{n+1/2} - g_{j+1/2} = U_{j-1}^{n+1/2}.$$

In any case, the contribution due to $+g_{j-1/2}$ pushes the resulting value back into the interior of the convex hull of the values $U_j^{n+1/2}$, $U_{j-1}^{n+1/2}$:

$$\begin{aligned} U_j^{n+1} &= U_j^{n+1/2} - g_{j+1/2} + g_{j-1/2} \\ &\overset{\text{worst case}}{=} \underbrace{U_{j-1}^{n+1/2} + \underbrace{g_{j-1/2}}_{\geq 0}}_{\in \operatorname{conv}\left(U_{j-1}^{n+1/2},\, U_j^{n+1/2}\right)} \\ &\leq U_{j-1}^{n+1/2} + \frac{\lambda}{2}\left(U_j^{n+1/2} - U_{j-1}^{n+1/2}\right) \\ &= \left(1 - \frac{\lambda}{2}\right) U_{j-1}^{n+1/2} + \frac{\lambda}{2} U_j^{n+1/2}, \end{aligned}$$

imposing the stability condition $\lambda \leq 2$ which is satisfied for the upwind scheme anyway. The other possible cases can be treated analogously, concluding the proof. □

Because of the properties of the minmod function, the core of the proof also works without the assumption (27). Thus we can give directly the desired

Corollary 3.1 (Global Maximum Principle). *The investigated scheme satisfies globally a discrete maximum principle.*

As indicated, the erosion process can be investigated analogously, yielding a global discrete minimum principle and a local discrete extremum principle.

4. The Two-Dimensional FCT Algorithm

Let us now extend the one-dimensional analysis of the preceding section to the two-dimensional case. Also here, we only discuss the dilation process in detail.

4.1. The General Upwind Scheme in 2-D

The basis of the 2-D algorithm is a straightforward extension of the 1-D scheme. Since the underlying PDE reads as

$$\partial_t u \;=\; \|\nabla u\|_2 \;=\; \sqrt{|\partial_x u|^2 + \left|\partial_y u\right|^2}, \tag{31}$$

which, notably, incorporates an additive splitting of the terms constituted solely on u_x and u_y, respectively, we can simply employ the corresponding *1-D* upwind expressions to obtain the basic *2-D* upwind scheme for dilation processes with a disc.

In order to define this scheme, let us give the abbreviations

$$\begin{aligned} dU_i^n &:= \frac{\lambda}{2}\left|U_{i+1,j}^n - U_{i-1,j}^n\right| + \frac{\lambda}{2}\left(U_{i+1,j}^n - U_{ij}^n\right) \\ &\quad -\frac{\lambda}{2}\left(U_{ij}^n - U_{i-1,j}^n\right), \end{aligned} \tag{32}$$

$$\begin{aligned} dU_j^n &:= \frac{\lambda}{2}\left|U_{i,j+1}^n - U_{i,j-1}^n\right| + \frac{\lambda}{2}\left(U_{i,j+1}^n - U_{ij}^n\right) \\ &\quad -\frac{\lambda}{2}\left(U_{ij}^n - U_{i,j-1}^n\right), \end{aligned} \tag{33}$$

$$\begin{aligned} &\Delta U_{i,j+1/2}^k := U_{i,j+1}^n - U_{ij}^k \quad \text{and} \\ &\Delta U_{i+1/2,j}^k := U_{i+1,j}^n - U_{ij}^k. \end{aligned} \tag{34}$$

Introducing then also

$$\mathcal{D}U_i^n := \begin{cases} 0 & \text{for } \Delta U_{i-1/2,j}^n \geq 0 \text{ and } \Delta U_{i+1/2,j}^n \leq 0, \\ dU_i^n & \text{else,} \end{cases} \tag{35}$$

$$\mathcal{D}U_j^n := \begin{cases} 0 & \text{for } \Delta U_{i,j-1/2}^n \geq 0 \text{ and } \Delta U_{i,j+1/2}^n \leq 0, \\ dU_j^n & \text{else,} \end{cases} \tag{36}$$

then the scheme reads

$$U_{ij}^{n+1} = U_{ij}^n + \sqrt{\left(\mathcal{D}U_i^n\right)^2 + \left(\mathcal{D}U_j^n\right)^2}. \tag{37}$$

For the scheme (37) again Proposition 3.1 holds, ensuring reasonable properties of the method.

As in the 1-D case, one can apply the method (37) without further modification, compare Fig. 1. However, as already indicated, any numerical solution is fairly blurred at the edges incorporated in an image. Note, that the rotational invariance of the scheme (37) is obvious due to the consideration of the *2-norm*.

For the application of a FCT strategy, it is crucial to observe that *there is no general way to extract the discrete viscosity terms out of the square root* in (37). This is exactly the reason why we have to go a different way which distinguishes our scheme from other FCT schemes in the multidimensional setting. Note also, that we can now understand that our proceeding in the 1-D case has the character of the treatment of a special case: in 1-D, the $\partial_y u$-type terms in (37) can be omitted, so that finally—after taking $\sqrt{(\cdot)^2}$—the discrete viscosity terms can be separated directly in an additive fashion from the second-order discretisation of $|\partial_x u|$.

4.2. The FCT Formulation

For the derivation of the FCT formulation it is only necessary to consider the non-maximum case of (37) as extrema will be detected automatically by the minmod-stabilisation, i.e., we have to treat

$$U_{ij}^{n+1} = U_{ij}^n + \sqrt{\left(dU_i^n\right)^2 + \left(dU_j^n\right)^2}, \tag{38}$$

in order to derive our 2-D FCT scheme for dilation.

Essential for the definition of our FCT procedure is to split a *viscous part* from a *second-order part*. Thus, we add zero in (38) obtaining

$$\begin{aligned} &U_{ij}^{n+1} \\ &= U_{ij}^n + \sqrt{\left(dU_i^n\right)^2 + \left(dU_j^n\right)^2} \\ &\quad + \sqrt{\left(\frac{\lambda}{2}\left|U_{i+1,j}^n - U_{i-1,j}^n\right|\right)^2 + \left(\frac{\lambda}{2}\left|U_{i,j+1}^n - U_{i,j-1}^n\right|\right)^2} \\ &\quad - \sqrt{\left(\frac{\lambda}{2}\left|U_{i+1,j}^n - U_{i-1,j}^n\right|\right)^2 + \left(\frac{\lambda}{2}\left|U_{i,j+1}^n - U_{i,j-1}^n\right|\right)^2}. \end{aligned} \tag{39}$$

Consequently, we now identify the viscous part as

$$-\sqrt{\left(\frac{\lambda}{2}\left|U_{i+1,j}^{n}-U_{i-1,j}^{n}\right|\right)^2+\left(\frac{\lambda}{2}\left|U_{i,j+1}^{n}-U_{i,j-1}^{n}\right|\right)^2} +\sqrt{\left(dU_i^n\right)^2+\left(dU_j^n\right)^2},$$

while

$$U_{ij}^{n+1} = U_{ij}^{n}+\sqrt{\left(\frac{\lambda}{2}\left|U_{i+1,j}^{n}-U_{i-1,j}^{n}\right|\right)^2+\left(\frac{\lambda}{2}\left|U_{i,j+1}^{n}-U_{i,j-1}^{n}\right|\right)^2}$$

defines the separated (spatial) second-order part.

Note that the viscous part is now nonlinear and it cannot be split up additively further into viscous fluxes due to the dimensional influence. For the FCT procedure, it must be handled as one block.

Analogously to (32), (33), we now introduce the abbreviations

$$g_{i+1/2,j} := \operatorname{minmod}\left(\Delta U_{i-1/2,j}^{n+1/2},\ \frac{\lambda}{2}\Delta U_{i+1/2,j}^{n+1/2},\ \Delta U_{i+3/2,j}^{n+1/2}\right), \tag{40}$$

$$g_{i,j+1/2} := \operatorname{minmod}\left(\Delta U_{i,j-1/2}^{n+1/2},\ \frac{\lambda}{2}\Delta U_{i,j+1/2}^{n+1/2},\ \Delta U_{i,j+3/2}^{n+1/2}\right). \tag{41}$$

Following then consequently the FCT strategy, we define

$$Q_h^{n+1/2} := \sqrt{\left(\frac{\lambda}{2}\left|U_{i+1,j}^{n+1/2}-U_{i-1,j}^{n+1/2}\right|\right)^2+\left(\frac{\lambda}{2}\left|U_{i,j+1}^{n+1/2}-U_{i,j-1}^{n+1/2}\right|\right)^2}, \tag{42}$$

$$Q_l^{n+1/2} := \sqrt{\left(\delta U_i^{n+1/2}\right)^2+\left(\delta U_j^{n+1/2}\right)^2}, \tag{43}$$

where the *stabilised backward diffusive fluxes* are incorporated by

$$\delta U_i^{n+1/2} := \frac{\lambda}{2}\left|U_{i+1,j}^{n+1/2}-U_{i-1,j}^{n+1/2}\right|+g_{i+1/2,j}-g_{i-1/2,j}, \tag{44}$$

$$\delta U_j^{n+1/2} := \frac{\lambda}{2}\left|U_{i,j+1}^{n+1/2}-U_{i,j-1}^{n+1/2}\right|+g_{i,j+1/2}-g_{i,j-1/2}, \tag{45}$$

and we correct the 2-D viscous basis scheme (37) by

$$U_{ij}^{n+1} = U_{ij}^{n+1/2}+Q_h^{n+1/2}-Q_l^{n+1/2} \tag{46}$$

using a notation analogously to the one in the preceding section.

We test our new FCT dilation scheme by considering the real-world test image from Fig. 5. As in the case documented by Fig. 1(d) the FCT dilation algorithm gives the desired sharp resolution.

4.3. Stability in 2-D

We now investigate the crucial stability properties of the method, meaning the validity of a *local extremum principle* and a *global discrete maximum principle*, respectively. As indicated, the major difficulty in the 2-D case is imposed by the nonlinearities due to the dimensional influence in (42)–(45).

Theorem 4.1 (Local Extremum Principle). *The described FCT dilation scheme (46) satisfies locally a discrete maximum–minimum principle.*

Proof: It is useful to introduce the abbreviations

$$\alpha_i := \frac{\lambda}{2}\left|U_{i+1,j}^{n+1/2}-U_{i-1,j}^{n+1/2}\right|, \quad \alpha_j := \frac{\lambda}{2}\left|U_{i,j+1}^{n+1/2}-U_{i,j-1}^{n+1/2}\right|, \tag{47}$$

$$\beta_i := g_{i+1/2,j}-g_{i-1/2,j}, \quad \beta_j := g_{i,j+1/2}-g_{i,j-1/2}, \tag{48}$$

for defining the vectors

$$\vec{\alpha} := \left(\alpha_i,\ \alpha_j\right)^T \quad \text{and} \quad \vec{\beta} := \left(\beta_i,\ \beta_j\right)^T. \tag{49}$$

Using (48)–(49), we can rewrite $Q_h^{n+1/2}$ and $Q_l^{n+1/2}$ from (42) and (43) as:

$$Q_h^{n+1/2} = \|\vec{\alpha}\|_2, \quad Q_l^{n+1/2} = \|\vec{\alpha}+\vec{\beta}\|_2, \tag{50}$$

Figure 5. (a) Left: Initial image, 256 × 256 pixels. (b) Right: Dilation computed by our new FCT scheme ($\Delta x = \Delta y = 1$, $\Delta t = 0.5$, 30 iterations).

and the updated formula (46) reads

$$U_{ij}^{n+1} = U_{ij}^{n+1/2} + \|\vec{\alpha}\|_2 - \|\vec{\alpha} + \vec{\beta}\|_2. \tag{51}$$

Concerning a further analysis of (51), let us point out that we have on the one hand

$$\begin{aligned} \|\vec{\alpha}\|_2 - \|\vec{\alpha} + \vec{\beta}\|_2 &= \|\vec{\alpha} + \vec{\beta} - \vec{\beta}\|_2 - \|\vec{\alpha} + \vec{\beta}\|_2 \\ &\le \|\vec{\alpha} + \vec{\beta}\|_2 + \|\vec{\beta}\|_2 - \|\vec{\alpha} + \vec{\beta}\|_2 \\ &= \|\vec{\beta}\|_2, \end{aligned} \tag{52}$$

while we can also easily deduce

$$\|\vec{\alpha}\|_2 - \|\vec{\alpha} + \vec{\beta}\|_2 \ge \|\vec{\alpha}\|_2 - (\|\vec{\alpha}\|_2 + \|\vec{\beta}\|_2) = -\|\vec{\beta}\|_2. \tag{53}$$

Assembling (52) and (53), we obtain

$$\left|\|\vec{\alpha}\|_2 - \|\vec{\alpha} + \vec{\beta}\|_2\right| \le \|\vec{\beta}\|_2. \tag{54}$$

For convenience, let us for the moment assume that

$$\operatorname{sign}\left(\Delta U_{i+1/2,j}^{n+1/2}\right) = \operatorname{sign}\left(\Delta U_{i-1/2,j}^{n+1/2}\right) \ne 0, \tag{55}$$

$$\operatorname{sign}\left(\Delta U_{i,j+1/2}^{n+1/2}\right) = \operatorname{sign}\left(\Delta U_{i,j-1/2}^{n+1/2}\right) \ne 0 \tag{56}$$

hold. Furthermore, let us consider local data maxima

$$\begin{aligned} &U_{i+1,j}^{n+1/2} > U_{ij}^{n+1/2} > U_{i-1,j}^{n+1/2} \quad \text{and} \\ &U_{i,j+1}^{n+1/2} > U_{ij}^{n+1/2} > U_{i,j-1}^{n+1/2}. \end{aligned} \tag{57}$$

By the construction of the flux function g, see (40) and (41), we can transfer directly the argument of the proof of Lemma 3.2 in order to see that $\|\vec{\beta}\|_2$ is limited by

$$\frac{\lambda}{2}\sqrt{\left(U_{i+1,j}^{n+1/2} - U_{ij}^{n+1/2}\right)^2 + \left(U_{i,j+1}^{n+1/2} - U_{ij}^{n+1/2}\right)^2}. \tag{58}$$

Taking the maximum out of the differences $\Delta U_{i+1/2,j}^{n+1/2}$ and $\Delta U_{i,j+1/2}^{n+1/2}$ occuring in (58), it follows that the antidiffusive flux contributions can be estimated via

$$\frac{\lambda}{2}\sqrt{2}\max\left(U_{i+1,j}^{n+1/2} - U_{ij}^{n+1/2},\ U_{i,j+1}^{n+1/2} - U_{ij}^{n+1/2}\right), \tag{59}$$

i.e., we obtain the validity of a local discrete maximum principle under the condition

$$\frac{\lambda}{2}\sqrt{2} \le 1 \quad \Leftrightarrow \quad \lambda \le \sqrt{2}$$

which is satisfied anyway by the CFL condition of the upwind scheme which reads in 2-D as $\lambda \le 1/\sqrt{2}$. □

Remarks

(a) Let us note that, by construction, the proof of Theorem 4.1 can easily be extended to higher dimensions.

(b) By our derivation of the algorithm and by the proof of Theorem 4.1, it is clear that the crucial restriction imposed on the time step size is due to the CFL condition for the upwind scheme, and not due to the antidiffusion step.

(c) The above procedure can easily be employed analogously for the erosion process, see Fig. 6 where we used the resulting 2-D FCT erosion scheme. Thus, for both dilation and erosion we obtain a discrete maximum–minimum principle as well as a global extremum principle, respectively.

Figure 6. Initial image (left) together with a snapshot of the erosion process with our FCT scheme, here with $\Delta x = \Delta y = 1$, $\Delta t = 0.5$, and 10 iterations.

Within Fig. 7 we demonstrate the convergence properties of the erosion scheme. We observe that the numerical errors vanish when refining the grid. Especially, the shape of the circle becomes more rotational invariant during the refinement process: this shows the consistency of the method to the underlying rotational invariant PDE.

We now test both the dilation/erosion schemes by means of two additional synthetical examples, see Figs. 8 and 9. By the square test we especially observe the role of the structure element, also, we see that the borders between different regions of grey values are very sharp.

The triangle experiment employs an integration up to $t = 2.5$, i.e., the result is a result where sub-pixel accuracy is mandatory. Also here, we see the influence of the structure element and the sharp resolution of our method.

5. Summary and Conclusions

We have presented a novel FCT type algorithm for morphological dilation and erosion processes with a disc as structuring element. It features the desirable properties of *rotational invariance* and *sharp resolution*. Moreover, the algorithm can easily be extended to a higher-dimensional setting while retaining these qualities. Technically, we have employed an unconventional nonlinear genuinely multidimensional formulation of antidiffusive fluxes in order to achieve these goals. The resolution of the new method outperforms the Rouy-Tourin and Osher-Sethian schemes that are frequently used in PDE-based mathematical morphology. Compared to other FCT approaches the scheme is competitive, while we rely on the discretisation of the underlying PDE. Our work has addressed the main shortcoming of PDE-based morphological algorithms and makes their resolution at shock fronts comparable to set-based morphological schemes.

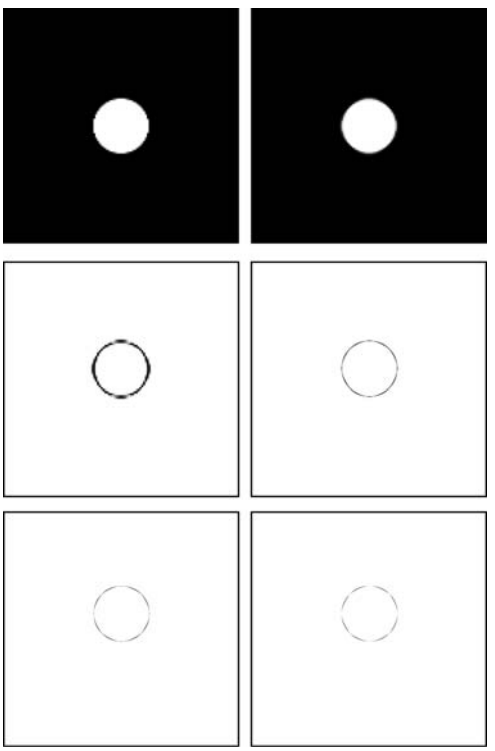

Figure 7. Top row: Exact erosion solution (left) of the disc displayed in Fig. 1 (a), together with (right) numerically eroded disc by our FCT scheme with $\Delta x = \Delta y = 1$, $\Delta t = 0.5$, and 20 iterations. Middle row: Rescaled difference mappings. (Left) Between the above figures. (Right) Between corresponding figures where the solution is computed on a finer grid, $\Delta x = \Delta y = 0.25$. Bottom row: Rescaled difference mappings of further refinements. (Left) For $\Delta x = \Delta y = 0.125$. (Right) For $\Delta x = \Delta y = 0.03125$.

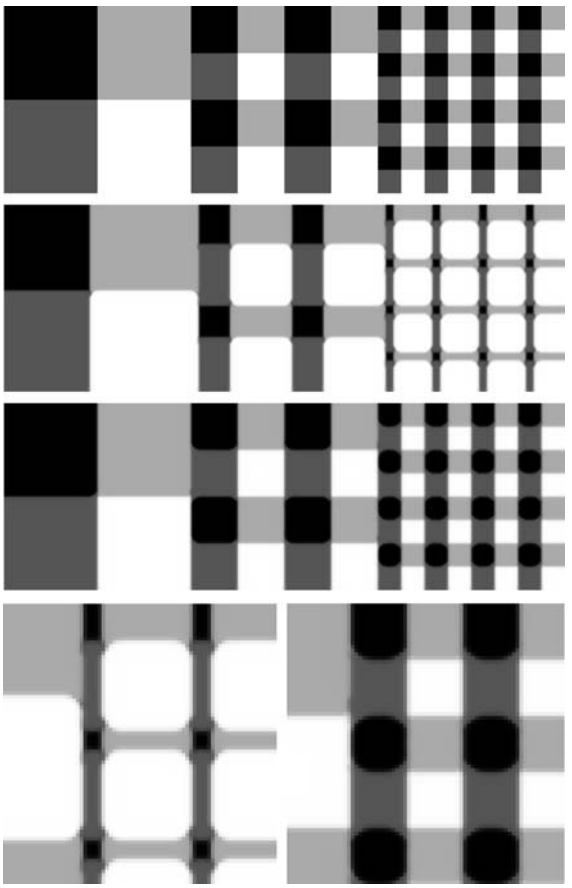

Figure 8. Top: Initial image, 120×360 pixels. 2nd from top: Dilation computed by our new FCT scheme ($\Delta x = \Delta y = 1$, $\Delta t = 0.5$, 10 iterations). 3rd from top: Erosion computed using the dilated image as initial condition (same parameters). Bottom left: Zoom into 2nd image from top. Bottom right: Zoom into 3rd image from top.

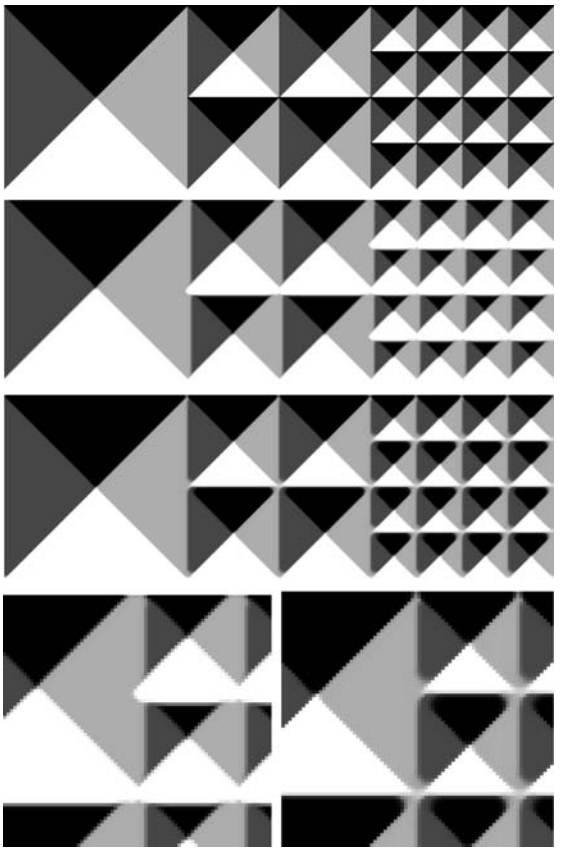

Figure 9. Top: Initial image, 120×360 pixels. 2nd from top: Dilation computed by our new FCT scheme ($\Delta x = \Delta y = 1$, $\Delta t = 0.5$, 5 iterations). 3rd from top: Erosion computed using the dilated image as initial condition (same parameters). Bottom left: Zoom into 2nd image from top. Bottom right: Zoom into 3rd image from top.

In our ongoing research we study extensions of this FCT appoach to morphological PDEs with other non-digitally scalable structuring elements such as ellipses.

Appendix

For the convenience of the interested reader, we give a brief compilation of the 2-D dilation/erosion algorithms.

The Dilation Algorithm

1. Predictor step with upwind scheme. Compute $U^{n+1/2}$ from U^n according to (37) with $\Delta t \leq 1/\sqrt{2}$.
2. Corrector step with stabilised inverse diffusion scheme. Compute U^{k+1} from $U^{k+1/2}$ by (46), thereby assembling the ingredients (40), (41), (44), (45) within (42) and (43).

The Erosion Algorithm

1. Predictor step with upwind scheme, using instead of (37) but by the same stability condition as for the dilation scheme:

$$\mathcal{D}U_i^n := \begin{cases} 0 & \text{for } \Delta U_{i-1/2,j}^n \leq 0 \text{ and } \Delta U_{i+1/2,j}^n \geq 0, \\ dU_i^n & \text{else,} \end{cases}$$

$$\mathcal{D}U_j^n := \begin{cases} 0 & \text{for } \Delta U_{i,j-1/2}^n \leq 0 \text{ and } \Delta U_{i,j+1/2}^n \geq 0, \\ dU_j^n & \text{else,} \end{cases}$$

$$
\begin{aligned}
dU_i^n &:= \frac{\lambda}{2}\left|U_{i+1,j}^n - U_{i-1,j}^n\right| - \frac{\lambda}{2}\left(U_{i+1,j}^n - U_{ij}^n\right) \\
&\quad + \frac{\lambda}{2}\left(U_{ij}^n - U_{i-1,j}^n\right), \\
dU_j^n &:= \frac{\lambda}{2}\left|U_{i,j+1}^n - U_{i,j-1}^n\right| - \frac{\lambda}{2}\left(U_{i,j+1}^n - U_{ij}^n\right) \\
&\quad + \frac{\lambda}{2}\left(U_{ij}^n - U_{i,j-1}^n\right). \\
U_{ij}^{n+1} &= U_{ij}^n - \sqrt{\left(\mathcal{D}U_i^n\right)^2 + \left(\mathcal{D}U_j^n\right)^2}.
\end{aligned}
$$

2. Corrector step with stabilised inverse diffusion scheme. Compute U^{k+1} from $U^{k+1/2}$ by (46), using the definitions

$$
\begin{aligned}
Q_h^{n+1/2} &:= \\
&-\sqrt{\left(\frac{\lambda}{2}\left|U_{i+1,j}^{n+1/2} - U_{i-1,j}^{n+1/2}\right|\right)^2 + \left(\frac{\lambda}{2}\left|U_{i,j+1}^{n+1/2} - U_{i,j-1}^{n+1/2}\right|\right)^2}, \\
Q_l^{n+1/2} &:= -\sqrt{\left(\delta U_i^{n+1/2}\right)^2 + \left(\delta U_j^{n+1/2}\right)^2}, \\
\delta U_i^{n+1/2} & \\
&:= \frac{\lambda}{2}\left|U_{i+1,j}^{n+1/2} - U_{i-1,j}^{n+1/2}\right| - g_{i+1/2,j} + g_{i-1/2,j}, \\
\delta U_j^{n+1/2} & \\
&:= \frac{\lambda}{2}\left|U_{i,j+1}^{n+1/2} - U_{i,j-1}^{n+1/2}\right| - g_{i,j+1/2} + g_{i,j-1/2}.
\end{aligned}
$$

Acknowledgments

The authors gratefully acknowledge the financial support of their work by the *Deutsche Forschungsgemeinschaft (DFG)* under the grants SO 363/9-1 and WE 2602/1-2.

Notes

1. ENO means *essentially non-oscillatory*. By adapting the stencil for derivative approximations to the local smoothness of the solution, ENO schemes obtain both high-order accuracy in smooth regions and sharp shock transitions.
2. The Courant–Friedrichs–Lewy (CFL) condition is the fundamental stability criterion for numerical schemes for hyperbolic PDEs. It requires that the numerical domain of dependence is included in the analytical domain of dependence of the PDE [11, 21]. For the case of the uwind schemes (10) and (11) introduced above, the CFL condition reads $\Delta t \max |f'(U_j^n)| \leq \Delta x$, where the maximum is computed over the set $\{U_j^n\}$ of all given data.
3. An entropy solution is a specific generalised solution, since classical, differentiable solutions are inappropriate to admit discontinuities that are characteristic for hyperbolic conservation laws.

References

1. L. Alvarez, F. Guichard, P.-L. Lions, and J.-M. Morel, "Axioms and fundamental equations in image processing," *Archive for Rational Mechanics and Analysis*, Vol. 123, pp. 199–257, 1993.
2. A.B. Arehart, L. Vincent, and B.B. Kimia, "Mathematical morphology: The Hamilton–Jacobi connection," in *Proc. Fourth International Conference on Computer Vision*, Berlin. IEEE Computer Society Press, May 1993, pp. 215–219.
3. J.P. Boris and D.L. Book, "Flux corrected transport. I. SHASTA, a fluid transport algorithm that works," *Journal of Computational Physics*, Vol. 11, No. 1, pp. 38–69, 1973.
4. J.P. Boris and D.L. Book. "Flux corrected transport. III. Minimal error FCT algorithms," *Journal of Computational Physics*, Vol. 20, pp. 397–431, 1976.
5. J.P. Boris, D.L. Book, and K. Hain, "Flux corrected transport. II. Generalizations of the method," *Journal of Computational Physics*, Vol. 18, pp. 248–283, 1975.
6. M. Breuß, "An analysis of discretisations of inverse diffusion equations," To appear in *Computing Letters*.
7. M. Breuß, T. Brox, T. Sonar, and J. Weickert, "Stabilized nonlinear inverse diffusion for approximating hyperbolic PDEs," in *Scale-Space and PDE Methods in Computer Vision*, R. Kimmel, N. Sochen, and J. Weickert (Eds.), Vol. 3459 of *Lecture Notes in Computer Science*, Springer, Berlin, 2005, pp. 536–547.
8. R.W. Brockett and P. Maragos, "Evolution equations for continuous-scale morphology," in *Proc. IEEE International Conference on Acoustics, Speech and Signal Processing*, Vol. 3, San Francisco, CA, Mar. 1992, pp. 125–128.
9. R.W. Brockett and P. Maragos, "Evolution equations for continuous-scale morphological filtering," *IEEE Transactions on Signal Processing*, Vol. 42, No. 12, pp. 3377–3386, 1994.
10. M.A. Butt and P. Maragos, "Comparison of multiscale morphology approaches: PDE implemented via curve evolution versus Chamfer distance transform," in *Mathematical Morphology and its Applications to Image and Signal Processing*, P. Maragos, R.W. Schafer, and M.A. Butt (Eds.), Vol. 5 of *Computational Imaging and Vision*, Kluwer: Dordrecht, 1996, pp. 31–40.
11. R. Courant, K. Friedrichs, and H. Lewy, "Über die partiellen differenzengleichungen der mathematischen Physik," *Mathematische Annalen*, Vol. 100, pp. 32–74, 1928.
12. E.R. Dougherty, *Mathematical Morphology in Image Processing*. Marcel Dekker: New York, 1993.
13. L.C. Evans, *Partial Differential Equations*, Vol. 19 of *Graduate Studies in Mathematics*. American Mathematical Society, Providence, 1998.
14. S.J. Farlow, *Partial Differential Equations for Scientists and Engineers*. Dover: New York, 1993.
15. E. Godlewski and P.-A. Raviart, *Hyperbolic Systems of Conservation Laws*. Edition Marketing, 1991.
16. J. Goutsias, L. Vincent, and D.S. Bloomberg (Eds.), *Mathematical Morphology and its Applications to Image and Signal Processing*, Vol. 18 of *Computational Imaging and Vision*. Kluwer: Dordrecht, 2000.
17. H.J.A.M. Heijmans, *Morphological Image Operators*. Academic Press: Boston, 1994.
18. H.J.A.M. Heijmans and J.B.T.M. Roerdink (Eds.), *Mathematical Morphology and its Applications to Image and Signal Processing*, Vol. 12 of *Computational Imaging and Vision*. Kluwer: Dordrecht, 1998.

19. D. Kuzmin, R. Löhner, and S. Turek (Eds.), *Flux-Corrected Transport*. Springer: Berlin, 2005.
20. D. Kuzmin and S. Turek, "Flux correction tools for finite elements," *Journal of Computational Physics*, Vol. 175, pp. 525–558, 2002.
21. R.J. LeVeque, *Finite Volume Methods for Hyperbolic Problems*. Cambridge University Press: Cambridge, UK, 2002.
22. P. Maragos, "Partial differential equations for morphological scale-spaces and eikonal applications," in *The Image and Video Compression Handbook*, 2nd edn., A.C. Bovik, Elsevier Academic Press, 2005, pp. 587–612.
23. P. Maragos, R.W. Schafer, and M.A. Butt (Eds.), *Mathematical Morphology and its Applications to Image and Signal Processing*, Vol. 5 of *Computational Imaging and Vision*. Kluwer: Dordrecht, 1996.
24. G. Matheron, *Random Sets and Integral Geometry*. Wiley: New York, 1975.
25. S. Osher and R.P. Fedkiw, *Level Set Methods and Dynamic Implicit Surfaces*, Vol. 153 of *Applied Mathematical Sciences*. Springer: New York, 2002.
26. S. Osher and J.A. Sethian, "Fronts propagating with curvature-dependent speed: Algorithms based on Hamilton–Jacobi formulations," *Journal of Computational Physics*, 79:12–49, 1988.
27. C. Ronse, L. Najman, and E. Decencière (Eds.), *Mathematical Morphology: 40 Years On*, Vol. 30 of *Computational Imaging and Vision*. Springer: Dordrecht, 2005.
28. E. Rouy and A. Tourin, "A viscosity solutions approach to shape-from-shading," *SIAM Journal on Numerical Analysis*, Vol. 29, pp. 867–884, 1992.
29. G. Sapiro, R. Kimmel, D. Shaked, B.B. Kimia, and A.M. Bruckstein, "Implementing continuous-scale morphology via curve evolution," *Pattern Recognition*, Vol. 26, pp. 1363–1372, 1993.
30. M. Schmitt and J. Mattioli, *Morphologie mathématique*. Masson: Paris, 1993.
31. J. Serra, *Image Analysis and Mathematical Morphology*, Vol. 1. Academic Press: London, 1982.
32. J. Serra. *Image Analysis and Mathematical Morphology*, Vol. 2. Academic Press: London, 1988.
33. J. Serra and P. Salembier (Eds.), *Proc. Internationanal Workshop on Mathematical Morphology and its Applications to Signal Processing*. Barcelona, Spain, May 1993.
34. J. Serra and P. Soille (Eds.), *Mathematical Morphology and its Applications to Image Processing*, Vol. 2 of *Computational Imaging and Vision*. Kluwer: Dordrecht, 1994.
35. J.A. Sethian, *Level Set Methods and Fast Marching Methods 2nd edn.*. Cambridge University Press: Cambridge, UK, 1999. aperback edition.
36. K. Siddiqi, B.B. Kimia, and C.W. Shu, "Geometric shock-capturing ENO schemes for subpixel interpolation, computation and curve evolution," *Graphical Models and Image Processing*, Vol. 59, pp. 278–301, 1997.
37. P. Soille, *Morphological Image Analysis 2nd edn.*. Springer, Berlin, 2003.
38. P. Stoll, C. Shu, and B.B. Kimia, "Shock-capturing numerical methods for viscosity solutions of certain PDEs in computer vision: The Godunov, Osher–Sethian and ENO schemes," Technical Report LEMS-132, Division of Engineering, Brown University, Providence, RI, 1994.
39. H. Talbot and R. Beare (Eds.), in *Proc. Sixth International Symposium on Mathematical Morphology and its Applications*. Sydney, Australia, April 2002. http://www.cmis.csiro.au/ismm2002/proceedings/.
40. R. van den Boomgaard, "Mathematical morphology: extensions towards computer vision," PhD thesis, University of Amsterdam, The Netherlands, 1992.
41. R. van den Boomgaard, "Numerical solution schemes for continuous-scale morphology," in *Scale-Space Theories in Computer Vision*, M. Nielsen, P. Johansen, O.F. Olsen, and J. Weickert (Eds.), Vol. 1682 of *Lecture Notes in Computer Science*, Springer: Berlin, 1999, pp. 199–210.
42. S.T. Zalesak, "Fully multidimensional flux-corrected transport algorithms for fluids," *Journal of Computational Physics*, Vol. 31, pp. 335–362, 1979.
43. S.T. Zalesak, "Introduction to "Flux corrected transport. I. SHASTA, a fluid transport algorithm that works," *Journal of Computational Physics*, Vol. 135, pp. 170–171, 1997.

Michael Breuß received his diploma and Ph.D. degrees in mathematics from the University of Hamburg in 1998 and 2001, respectively. He worked as an assistant professor at the University of Hamburg, as post-doctoral researcher at the University of Bordeaux 1 and as a researcher at the Technical University Braunschweig. Since April 2006, he is an assistant professor at the Mathematical Image Analysis group at the Saarland University. His research interests are centered around numerical methods for partial differential equations, hyperbolic conservation laws and visual computing.

Joachim Weickert received his diploma and Ph.D. degrees in mathematics from the University of Kaiserslautern (Germany) in 1991 and 1996, respectively. In 2001 he obtained a habilitation degree in computer science from the University of Mannheim (Germany). He worked as research assistant at the University of Kaiserslautern, as post-doctoral researcher at the universities of Utrecht (The Netherlands) and Copenhagen (Denmark), and as assistant professor at the University of Mannheim. Currently he is full professor of mathematics and computer science at Saarland University in Saarbrücken (Germany), where he heads the Mathematical Image Analysis Group. His research interests include image processing, computer vision, and scientific computing.